International Journal of Solids and Structures 47 (2010) 1099–1107

Contents lists available at ScienceDirect

International Journal of Solids and Structures

journal homepage: www.elsevier.com/locate/ijsolstr

Stress concentrations in fractured compact bone simulated with a special class of anisotropic gradient elasticity

Inna M. Gitman [a,*], Harm Askes [b], Ellen Kuhl [c], Elias C. Aifantis [d,e]

[a] University of Sheffield, Department of Mechanical Engineering, Mappin Street, Sheffield S1 3JD, United Kingdom
[b] University of Sheffield, Department of Civil and Structural Engineering, Mappin Street, Sheffield S1 3JD, United Kingdom
[c] Stanford University, Mechanical Engineering, Building 530, 440 Escondido Mall, Stanford, CA 94305-3030, USA
[d] Aristotle University of Thessaloniki, Laboratory of Mechanics and Materials, Thessaloniki 54006, Greece
[e] Michigan Technological University, Center for Mechanics of Materials and Instabilities, Houghton, MI 49931, USA

ARTICLE INFO

Article history:
Received 11 May 2009
Received in revised form 17 November 2009
Available online 11 December 2009

Keywords:
Anisotropic gradient elasticity
Bone fracture
Bone stress concentrations

ABSTRACT

A new format of anisotropic gradient elasticity is formulated and implemented to simulate stress concentrations in cortical bone. The higher-order effect of the underlying microstructure in cortical bone is accounted for through the introduction of two length scale parameters and associated strain gradient terms which modify the response of the standard elastic macroscopic continuum: one internal length related to the longitudinal fibres and the other related to the transversal Haversian systems. Thus, anisotropic material behaviour is not only included in the anisotropy of the elastic effective stiffness properties, but also in the anisotropic sources of heterogeneity. The model is validated numerically in tests with bone fractures in the longitudinal and the transversal directions. It was found that the dominant length scale effects are those that coincide with the direction of fracture, as defined by the orientation of a pre-existing crack.

1. Introduction

Bones, as most biological tissues, are deformable organs with a complex internal microstructure. The mineralized osseous tissue, also called bone tissue, is one of the bone structural components. It gives bone its honeycomb-like three-dimensional microstructure. The two types of osseous tissue, spongy (or trabecular) and compact (or cortical), are biologically identical; however they have differently arranged microstructures. The microstructure of bone influences its mechanical response; for example the stress concentrations around fractures. The accurate description of the stress field around cracks in bone is crucial for making predictions on further crack growth or bone regrowth. It would be advantageous for diagnosis if a simple, linear elastic analysis of the fractured bone can be used to predict stress concentrations. Unfortunately, the classical equations of linear elasticity lead to singular stresses at the tips of sharp cracks. This is commonly ascribed to the lack of microstructural information in classical elasticity.

In order to describe the mechanical behaviour of complex structures such as human bones and take into account the information from the different levels of observation, multiscale modelling techniques should be used. Several multiscale modelling strategies exist. A straightforward, but computationally intensive approach is to model each individual microstructural detail. Alternatively, and more efficiently, the effects of the microstructure can be captured using enriched continuum theories on the macro-level, whereby the information of the lower level is appearing in the form of some additional terms and associated parameters in the constitutive relation. One of the examples of such enriched continuum theories used for bone modelling is the Cosserat theory, as discussed, for example, in (Fatemi et al., 2002; Kirchner and Lazar, 2008 and references quoted therein (see also Lakes, 1983, 1986). The other methodology which has been used here, is the theory of *gradient elasticity* (Mindlin, 1964; Mindlin and Eshel, 1968; Altan and Aifantis, 1997; Lazar et al., 2005). Compared to the classical theory of elasticity, additional spatial gradients (e.g. of the strain or the stress tensor itself and/or the void space in the case of a porous elastic material) of relevant state variables appear that are accompanied by internal length parameters which are assumed to represent the underlying microstructure. In its simpler form gradient elasticity involves one additional term, the Laplacian of a Hookean-like stress in the standard stress–strain law of classical elasticity (Aifantis, 1992). Of particular significance for the modelling of fracture is the capability of gradient elasticity to simulate stresses and strains around the tips of sharp cracks without the singularities that appear in classical elasticity (see, for example, Ru and Aifantis, 1993; Altan and Aifantis, 1997 for the first preliminary considerations on this topic). In this connection it is also remarked that gradient elasticity has also been used (Aifantis, 1999)

* Corresponding author.
E-mail address: i.gitman@sheffield.ac.uk (I.M. Gitman).

0020-7683/$ - see front matter © 2009 Elsevier Ltd. All rights reserved.
doi:10.1016/j.ijsolstr.2009.11.020

to model size effects in bone more efficiently than corresponding efforts through Cosserat theory (Lakes, 1983, 1986).

Several gradient elasticity formulations have been proposed in the literature. Aifantis and coworkers formulated a constitutive relation in which the stresses are related to the strains and to the second gradient of the strains (Ru and Aifantis, 1993; Aifantis, 1992; Altan and Aifantis, 1997; Lazar et al., 2005). It was also shown that the governing equations can be factorised using the Ru–Aifantis theorem, by which the fourth-order governing differential equations can be decoupled into two sets of second-order equations (Ru and Aifantis, 1993). This can be done in terms of displacements, strains or stresses (Askes et al., 2008) and greatly simplifies analytical and numerical solution procedures. A different formulation of a gradient-type elasticity was deduced earlier by Eringen from an integral-type nonlocal formulation of elasticity (Eringen, 1983; see also Altan and Aifantis, 1997). In this format, the stresses and their second gradients are related to the strains, and a similar strain-based formulation was studied in (Askes and Gutiérrez, 2006). The relation between these two formulations was earlier explored in (Askes and Aifantis, 2002) and they were denoted as "explicit" and "implicit", respectively — this terminology indicates that the former can be expressed as differential equations in which the displacements are the only unknowns, whereas the latter contains coupled differential equations where displacements are unknowns together with either stresses or strains.

Both types of the aforementioned gradient elasticity theories are equipped with an additional material parameter known as gradient coefficient or *internal length scale*. This length scale parameter carries the information from the lower scale and is related to its Representative Volume Element (RVE) size (Gitman et al., 2005). There exist several different methods in order to estimate the size of this RVE, see for instance (Gitman et al., 2007; Bažant and Novák, 2003; Drugan and Willis, 1996; Ren and Zheng, 2002). However, these methods are generally designed for isotropic materials and, as a result, the dimensions of the RVE are equal in all three spatial directions. The internal length scale parameter is, in turn, also the same in all three directions. The mechanical description becomes much more complex once the material is no longer isotropic. Bones that have a fibre-like structure are just one example. In order to describe stress concentrations around fractures in such materials, we suggest to use *anisotropic gradient elasticity* models — the anisotropy in such models not only concerns the stiffness (or compliance) characteristics but also the anisotropy of the length scale parameters.

In the present paper we aim to simulate stress concentrations around fractures in bones and we will therefore employ gradient elasticity with stress gradients. The two models we will use are the Ru–Aifantis theory with stress gradients and the Eringen theory. We will discuss these two theories, and their subtle differences, in Section 2. Roughly speaking, the essential difference between the two formulations is the format of the equilibrium equation: in the Ru–Aifantis theory the stress term entering the equilibrium equation is the classical stress and in the Eringen theory the gradient-enriched stress is included in the equilibrium equation. In Section 3 we discuss the two aspects of anisotropy in the context of compact bone, namely anisotropy of the elastic moduli and anisotropy of the gradient enrichment. The finite element equations are given in Section 4, and in Section 5 we treat examples with transversal and longitudinal tibial fracture.

In concluding this introductory section we would like to re-iterate that the present article documents our first attempts to characterize bone with its characteristic locally transversely isotropic microstructure using a particular form of anisotropic gradient elasticity. More involved are formal theories of generalised anisotropic elasticity (including both gradient and nonlocal versions) can be found in the original treatments of Mindlin (1968) and Eringen (2002). A more recent work on Cosserat type generalised elasticity applied to bone mechanics was elegantly presented in (Kirchner and Lazar, 2008). In a sense, the present model may be viewed as a special case of the aforementioned anisotropic generalised elasticity theories; in particular of (Mindlin, 1968). However, our aim here was not generality, but robustness in relation to the complex fracture configurations considered in the present work. In order to obtain physical insight in the question we posed, simplicity in the constitutive structure is required.

2. Isotropic gradient elasticity

In order to introduce microstructural effects into the mechanical description of a material element and (simultaneously) remove the singularities which may occur in classical elasticity, gradient-enriched elasticity models can be used. Let us first consider the isotropic case. A simple format of gradient elasticity for the case of isotropy was introduced by Aifantis and coworkers (1992,1993, 1997). In fact, this format first proposed by Aifantis (1992,1994) was obtained for elastic nanomaterials considered as a mixture of two interpenetrating and elastically interacting continua: the *bulk* and the *grain boundary* phases. Even though it turned out that formally this model is a special case of Mindlin's 5-constants gradient elasticity theory (Mindlin, 1964; Mindlin and Eshel, 1968), it was not obvious at the outset, without any other additional physical considerations, which is appropriate choice of constants for reducing the general/complex theory to a simple/robust model. The stresses (total stress in the terminology of Lazar et al., 2005; Lazar and Maugin, 2005, Cauchy stress in the terminology of Aifantis, 1992) σ_{ij} are related not only to the strains ε_{kl} but also to the second gradient of the strains, that is

$$\sigma_{ij} = D_{ijkl}(\varepsilon_{kl} - \ell^2 \varepsilon_{kl,mm}) \tag{1}$$

where D_{ijkl} is the fourth-order elastic stiffness tensor and ℓ is an internal length parameter that is related to the dimension of the microstructural heterogeneities. In the case of anisotropic material, such as fibrous bone material, different values of length scales may be used in different directions, see also Section 3. Classical elasticity can be retrieved by taking $\ell = 0$. Eq. (1) is solved together with the equilibrium equations

$$\sigma_{ij,j} + b_i = 0 \tag{2}$$

where b_i are the body forces. The classical strain–displacement relation reads

$$\varepsilon_{kl} = \frac{1}{2}(u_{k,l} + u_{l,k}) \tag{3}$$

as usual. Combining Eqs. (1)–(3) leads to a system of partial differential equations as

$$D_{ijkl}(u_{k,jl} - \ell^2 u_{k,jlmm}) + b_i = 0 \tag{4}$$

where the symmetry of the tensor D_{ijkl} has been used. As the highest derivative in terms of the displacements u_k is of the fourth-order, it is required to use $\mathscr{C}^1$-continuous shape functions, implying that the displacements, as well as their first derivatives, are continuous throughout the domain of interest. This is quite restrictive for finite element implementations, and below we will treat two formulations of gradient elasticity that avoid these stringent continuity requirements.

2.1. Gradient elasticity formulation of Ru and Aifantis

In order to reduce the continuity requirement from $\mathscr{C}^1$ to $\mathscr{C}^0$ the Ru–Aifantis theorem can be used (Ru and Aifantis, 1993), i.e. it is possible to rewrite Eq. (4) as

$$D_{ijkl}(u_k - \ell^2 u_{k,mm})_{,jl} + b_i = 0 \tag{5}$$

Defining two sets of displacements $u_k^g = u_k$ and $u_k^c = u_k - \ell^2 u_{k,mm}$ as the gradient-dependent displacements and the classical displacements, Eq. (5) can be rewritten as a system of equations, namely

$$D_{ijkl}u_{k,jl}^c + b_i = 0 \tag{6}$$

$$u_k^g - \ell^2 u_{k,mm}^g = u_k^c \tag{7}$$

As a consequence of this operator split, Eq. (6) can be solved independently from, and prior to, Eq. (7). That is, the classical displacements u_k^c are resolved using the classical elasticity formulation of expression (6), after which u_k^c are used as input for Eq. (7), which is then used to solve for u^g. Note that both Eqs. (6) and (7) are second-order (in terms of u^c and u^g, respectively), and as such a $\mathscr{C}^0$-continuous interpolations are sufficient (Tenek and Aifantis, 2002; Askes et al., 2008).

Since the second equation is formulated in terms of displacements, this approach is referred to as the *displacement-based* Ru–Aifantis (or *u*-RA) approach. A *strain-based* Ru–Aifantis (ε-RA) approach was suggested in order to overcome the issue of interpretation of the variationally consistent natural boundary conditions (Gutkin and Aifantis, 1999; Gutkin, 2000; Askes et al., 2008; Aifantis, 2003). The ε-RA formulation is obtained by taking the derivatives of Eq. (7). This leads to the following system of equations:

$$D_{ijkl}u_{k,jl}^c + b_i = 0 \tag{8}$$

$$\varepsilon_{kl}^g - \ell^2 \varepsilon_{kl,mm}^g = \frac{1}{2}\left(u_{k,l}^c + u_{l,k}^c\right) \tag{9}$$

where $\varepsilon_{kl}^g = \frac{1}{2}(u_{k,l}^g + u_{l,k}^g)$ are the gradient-enriched strains.

A further manipulation of the above gradient elasticity model is possible by pre-multiplying Eq. (9) with the constitutive tensor D, which results in a system of equations as

$$D_{ijkl}u_{k,jl}^c + b_i = 0 \tag{10}$$

$$\sigma_{ij}^g - \ell^2 \sigma_{ij,mm}^g = D_{ijkl}u_{k,l}^c \tag{11}$$

where $\sigma_{ij}^g = D_{ijkl}\varepsilon_{kl}^g$ are the gradient-enriched stresses This *stress-based* Ru–Aifantis (or σ-RA) approach has been used to remove singularities from the stress field at dislocations lines (see, for example, Gutkin and Aifantis, 1999; Gutkin, 2000; Aifantis, 2003; also Lazar et al., 2005; Lazar and Maugin, 2005 and references quoted therein).

2.2. Gradient elasticity formulation of Eringen

An earlier format of gradient elasticity, not based on the theorems of Ru and Aifantis, is due to Eringen (1983). It bears some similarities to the σ-RA model since Eq. (11) is employed. However, a difference exists in the equilibrium equations, where the gradient-enriched stresses σ_{ij}^g are used instead of the stresses of classical elasticity $\sigma_{ij}^c \equiv D_{ijkl}u_{k,l}^c$. The system of equations thus reads

$$\sigma_{ij,j}^g + b_i = 0 \tag{12}$$

$$\sigma_{ij}^g - \ell^2 \sigma_{ij,mm}^g = D_{ijkl}u_{k,l}^c \tag{13}$$

The above system of Eqs. (12) and (13) constitutes a coupled system of equations — in contrast to the three formulations of Ru and Aifantis, it is now not possible to solve Eq. (12) first and Eq. (13) afterwards. In a 2D context, this can be seen as follows: Eq. (12) contains two equations whereas σ_{ij}^g has three components. Furthermore, Eq. (13) contains three equations, with three unknown components of σ_{ij}^g and two unknown components of u_i^c. Hence, a coupled system of five equations with five unknowns must be solved.

In (Askes and Gutiérrez, 2006) the continuum mechanics background and the implementational aspects of this model are treated. It was demonstrated that a $\mathscr{C}^0$-continuous implementation suffices for the discretisation of the two sets of unknowns, namely σ_{ij}^g and u_i^c. However, it was also shown that the interpolation polynomials of σ_{ij}^g and u_i^c cannot be chosen independently: σ_{ij}^g must be interpolated one polynomial order higher than u_i^c. This is in contrast to Eqs. (10) and (11), where the two interpolation spaces are unrelated and can be chosen as preferred by the user, equal interpolations generally being a convenient choice (Askes et al., 2008). In the remainder of this paper, we will use the *uncoupled formulation* of Eqs. (10) and (11) and the *coupled formulation* of Eqs. (12) and (13).

3. Bone tissue, anisotropic gradient activity and internal length scales

In this study, we focus on compact bone (also known as cortical bone). Compact bone is an extremely hard, layered and strongly anisotropic material. The micro-structural representation of compact bone depends on the direction of observation. In the cross-section of the bone, compact bone can be presented as a set of repeating *unit cells*, which are known as *Haversian systems*. Each cell is built up from concentric layers of mineralized matrix material (lamellae), which are deposited around a central canal (the Haversian canal) containing blood vessels and nerves that service the bone. On the other hand, in the axial direction, compact bone has a layered fiber-like structure. Here the direction perpendicular to the Haversian systems will be denoted as x_1, and x_2, x_3 are the axes in the plane of the Haversian systems (see Fig. 1).

3.1. Anisotropic elastic moduli

Mechanically speaking, compact bone is an anisotropic material. In order to model such a material, first of all, the anisotropy of the elastic stiffness coefficients must be taken into account. Experimental studies have been reported in (Rho, 1996; Hoffmeister et al., 2000). The experiments were based on ultrasonic velocity measurements of a representatively large amount of samples obtained from normal cortical bone removed from the right tibia of eight human cadavers. This has resulted in the following elastic stress–strain relation with a stiffness matrix **D** of dimension MPa:

$$\begin{bmatrix} \sigma_{22} \\ \sigma_{33} \\ \sigma_{11} \\ \sigma_{31} \\ \sigma_{12} \\ \sigma_{23} \end{bmatrix} = 10^3 \cdot \begin{bmatrix} 19.5 & 11.4 & 12.5 & 0 & 0 & 0 \\ 11.4 & 20.1 & 12.5 & 0 & 0 & 0 \\ 12.5 & 12.5 & 30.9 & 0 & 0 & 0 \\ 0 & 0 & 0 & 5.72 & 0 & 0 \\ 0 & 0 & 0 & 0 & 5.17 & 0 \\ 0 & 0 & 0 & 0 & 0 & 4.05 \end{bmatrix} \begin{bmatrix} \varepsilon_{22} \\ \varepsilon_{33} \\ \varepsilon_{11} \\ \gamma_{31} \\ \gamma_{12} \\ \gamma_{23} \end{bmatrix} \tag{14}$$

As it was stated above, on the one hand compact bone has a layered fibrous structure and on the other hand it has a repeating Haversian cells structure. It is reasonable then to model compact bone as a transversely isotropic material. As a further approximation we will limit our study to the "plane strain" case within the x_1x_2-plane. As such, the stiffness matrix used in our computations is

$$\mathbf{D} = \begin{bmatrix} 19.5 & 12.5 & 0 \\ 12.5 & 30.9 & 0 \\ 0 & 0 & 5.17 \end{bmatrix} \cdot 10^3 \text{ MPa} \tag{15}$$

3.2. Anisotropic heterogeneity

Even with the aforementioned approximations, modelling compact bone must account for the fact that the underlying microstructure is different in different directions. As a consequence, different length scale parameters have to be considered. Generally

speaking, two length scale parameters must be distinguished. In the axial direction of the bone, gradient activity is governed by a length scale ℓ_F following from the mechanics and geometry of fibers. In the cross-section of the bone, the mechanics and geometry of the Haversian systems may be captured by a length scale ℓ_H. One way to identify these parameters is to connect them to the Representative Volume Elements (RVEs) in the relevant directions (Gitman et al., 2005). However, as the task of actually quantifying the relevant length scale parameters (or their associated RVE sizes) is a tedious one, an approximation of some sort is highly desirable. The problem can be approached from two different viewpoints:

- *Longitudinal heterogeneity*: Since the length of the fibers is much larger than their cross-section, one can state that $\ell_F \gg \ell_H$ and as such the task is to consider only ℓ_F and let ℓ_H be zero. In other words, such an approach assumes that the fibers are the main source of heterogeneity and that the cross-sectional properties are taken as homogeneous;
- *Transversal heterogeneity*: Again using the fact that the length of the fibers is much larger than their radius, one can approximate them to be parallel to each other and consider such a material as homogeneous in the fiber direction. The RVE size of a homogeneous material is theoretically zero, by which $\ell_F = 0$ and the task is now reduced to consider ℓ_H. In this approach the cross-sectional heterogeneity is assumed to be dominant.

The two approaches represent two extreme viewpoints, and a more accurate modelling approach would probably have to include both length scale effects at the same time (although in general $\ell_F \neq \ell_H$). However, it is of interest to check the performance of the two more simplified models, obtained by considering only one length scale at a time. Thus, in this paper we will investigate both approaches.

3.3. Anisotropic gradient elasticity

In Mindlin (1972) introduced a theory of anisotropic gradient-enhanced elasticity where the gradient-enriched stress–strain relation was of the form (by neglecting, for simplicity, a term involving a fifth-order material tensor C_{ijklm})

$$\sigma_{ij} = D_{ijkl}\varepsilon_{kl} - C_{ijmkln}\varepsilon_{kl,mn} \tag{16}$$

Eq. (16) describes the case of general anisotropy and C_{ijklmn} is a general sixth-order tensor that incorporates anisotropic elastic moduli effects, as well as anisotropic length scale effects. We wish to separate the two effects of anisotropy in a transparent manner, that is the anisotropy in the elastic moduli, as discussed in Section 3.1, and the anisotropy of gradient activity, which we will discuss in this section. To this end, we write the sixth-order tensor C_{ijklmn} as a combination of a fourth-order tensor with elastic moduli D_{ijkl} and a second-order tensor with length scale effects L_{mn}. Thus,

$$C_{ijmkln} = D_{ijkl}L_{mn} \tag{17}$$

with the transverse isotropy entering via the special form of the stiffness matrix D_{ijkl}, while L_{mn} in Eq. (17) is a second-order length scale tensor. Now, Eq. (16) can be rewritten as

$$\sigma_{ij} = D_{ijkl}(\varepsilon_{kl} - L_{mn}\varepsilon_{kl,mn}) \tag{18}$$

Transverse isotropy of the gradient activity is brought in via the relation

$$L_{mn} = \ell_F^2 n_m n_n + \ell_H^2(\delta_{mn} - n_m n_n) \tag{19}$$

where ℓ_F and ℓ_H are the length scales related to the specific direction of anisotropy defined by the unit vector n_i and the direction orthogonal to it. Furthermore, with the special condition of $\ell_F = \ell_H = \ell$, the case of isotropic gradient activity is recovered.

Now the equilibrium equation can be presented as

$$D_{ijkl}(u_k - L_{mn}u_{k,mn})_{,jl} + b_i = 0 \tag{20}$$

Identifying two sets of displacements $u_k^g = u_k$ and $u_k^c = u_k - L_{mn}u_{k,mn}$ as the gradient-dependent displacements and the classical displacements, Eq. (20) can be rewritten as a system of equations, namely

$$D_{ijkl}u^c_{k,jl} + b_i = 0 \tag{21}$$

$$u_k^g - L_{mn}u^g_{k,mn} = u_k^c \tag{22}$$

In terms of stresses, Eqs. (10) and (11) may now be written as

$$D_{ijkl}u^c_{k,jl} + b_i = 0 \tag{23}$$

$$\sigma_{ij}^g - L_{mn}\sigma^g_{ij,mn} = D_{ijkl}u^c_{k,l} \tag{24}$$

In his book (Eringen, 2002), Eringen has also introduced anisotropic nonlocality, although in a slightly different manner. In this paper we will use the particularisation of the Mindlin formalism for both the uncoupled Aifantis theory and the coupled Eringen theory. The coupled model with anisotropic gradient activity is thus written as

$$D_{ijkl}u^g_{k,jl} + b_i = 0 \tag{25}$$

$$\sigma_{ij}^g - L_{mn}\sigma^g_{ij,mn} = D_{ijkl}u^c_{k,l} \tag{26}$$

which replace Eqs. (12) and (13) valid for the case of isotropic gradient activity only.

4. Finite element equations

As mentioned above, we will model the anisotropy of bone taking the x_1 axis aligned with the specific direction of anisotropy. Now, substituting Eq. (19) into Eq. (24) or Eqs. (26) and (24) in the uncoupled formulation and Eq. (26) in the coupled formulation can each be replaced by

$$\sigma_{ij}^g - \ell_F^2 n_m n_n \sigma^g_{ij,mn} - \ell_H^2\left(\sigma^g_{ij,11} + \sigma^g_{ij,22}\right) + \ell_H^2 n_m n_n \sigma^g_{ij,mn} = D_{ijkl}u^c_{k,l} \tag{27}$$

here n_i are the components of a unit vector of the direction of anisotropy and orthogonal direction. As mentioned in Section 3, x_1 is aligned with the direction of anisotropy as such the components of the unit vector can take values $n = [1\ 0]$. Thus Eq. (27) can then be rewritten as

$$\sigma_{ij}^g - \ell_F^2\sigma^g_{ij,11} - \ell_H^2\sigma^g_{ij,22} = D_{ijkl}u^c_{k,l} \tag{28}$$

In a Galerkin formulation, the weak form of Eq. (28) is integrated by parts and boundary integrals appear as a result. These must be evaluated using boundary conditions. We will use here Neumann conditions, which are given as normal derivatives of the stresses on the boundaries. These derivatives of the stresses, multiplied with length scale coefficients, can also be interpreted as double stresses (Mindlin, 1964)

Both the uncoupled (σ-RA) and coupled gradient elasticity formulations contain stresses and displacements as the fundamental unknowns. The stresses and displacements are discretised with shape functions $\mathbf{N}_\sigma$ and $\mathbf{N}_u$, respectively. The discretised systems of equations can then be written in matrix–vector notation as

$$\text{uncoupled}: \int \begin{bmatrix} \left(\mathbf{N}_\sigma^T\mathbf{C}\mathbf{N}_\sigma + \ell_F^2\frac{\partial\mathbf{N}_\sigma^T}{\partial x_1}\mathbf{C}\frac{\partial\mathbf{N}_\sigma}{\partial x_1} + \ell_H^2\frac{\partial\mathbf{N}_\sigma^T}{\partial x_2}\mathbf{C}\frac{\partial\mathbf{N}_\sigma}{\partial x_2}\right) & -\mathbf{N}_\sigma^T\mathbf{B}_u \\ \mathbf{0} & \mathbf{B}_u^T\mathbf{D}\mathbf{B}_u \end{bmatrix} \mathrm{d}V \begin{bmatrix}\boldsymbol{\Sigma}\\ \mathbf{U}\end{bmatrix} = \begin{bmatrix}\mathbf{0}\\ \mathbf{f}\end{bmatrix} \tag{29}$$

$$\text{coupled}: \int \begin{bmatrix} \left(\mathbf{N}_\sigma^T\mathbf{C}\mathbf{N}_\sigma + \ell_F^2\frac{\partial\mathbf{N}_\sigma^T}{\partial x_1}\mathbf{C}\frac{\partial\mathbf{N}_\sigma}{\partial x_1} + \ell_H^2\frac{\partial\mathbf{N}_\sigma^T}{\partial x_2}\mathbf{C}\frac{\partial\mathbf{N}_\sigma}{\partial x_2}\right) & -\mathbf{N}_\sigma^T\mathbf{B}_u \\ -\mathbf{B}_u^T\mathbf{N}_\sigma & \mathbf{0} \end{bmatrix} \mathrm{d}V \begin{bmatrix}\boldsymbol{\Sigma}\\ \mathbf{U}\end{bmatrix} = \begin{bmatrix}\mathbf{0}\\ -\mathbf{f}\end{bmatrix} \tag{30}$$

where $\mathbf{C} \equiv \mathbf{D}^{-1}$ is the compliance matrix, $\mathbf{f}$ is the external force vector, and $\boldsymbol{\Sigma}$ and $\mathbf{U}$ are the nodal values of σ_{ij}^g and u_i^c, respectively.

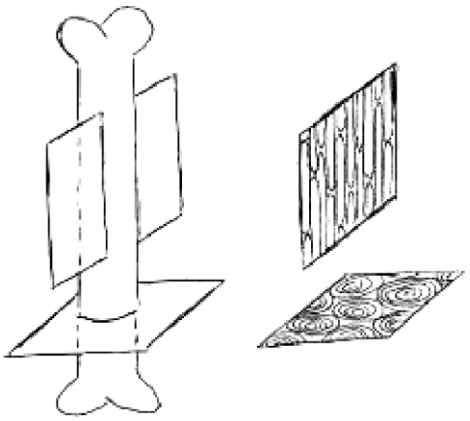

Fig. 1. Bone and its cross-sections: longitudinal direction (top-right) and transversal (bottom-right).

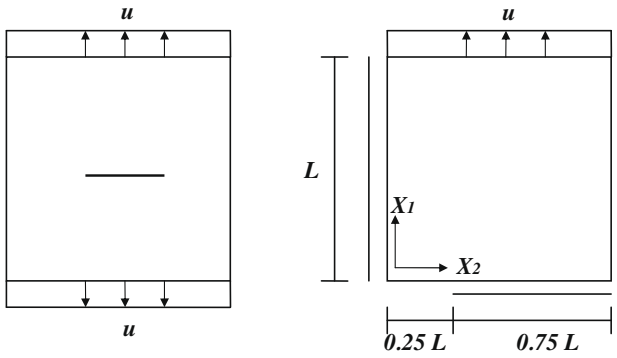

Fig. 2. Bone with transversal fracture – geometry of the specimen (left), dimensions and loading conditions of modelled top-right quarter (right).

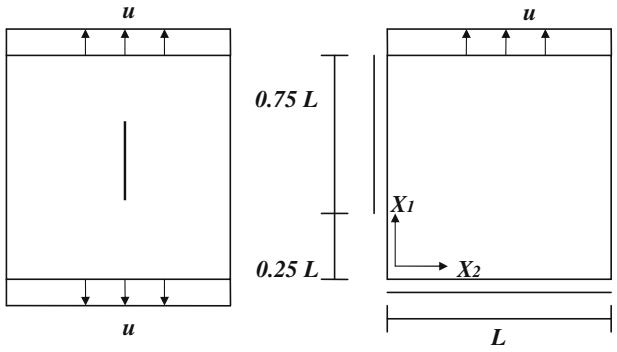

Fig. 3. Bone with longitudinal fracture – geometry of the specimen (left), dimensions and loading conditions of modelled top-right quarter (right).

Furthermore, a coordinate system has been used whereby the x_1-axis is aligned with the bone axis and the fibers, while the x_2-axis is located in the cross-section of the bone. The shape function derivative matrix $\mathbf{B}_u$ is defined for a two-dimensional problem statement as

$$\mathbf{B}_u = \begin{bmatrix} \frac{\partial N_1}{\partial x_1} & 0 & \frac{\partial N_2}{\partial x_1} & 0 & \dots \\ 0 & \frac{\partial N_1}{\partial x_2} & 0 & \frac{\partial N_2}{\partial x_2} & \dots \\ \frac{\partial N_1}{\partial x_2} & \frac{\partial N_1}{\partial x_1} & \frac{\partial N_2}{\partial x_2} & \frac{\partial N_2}{\partial x_1} & \dots \end{bmatrix} \tag{31}$$

as usual. Note that the second row of Eq. (30) has been multiplied by -1 in order to obtain a symmetric system matrix. The first rows of Eqs. (29) and (30) also show the similarities between the uncoupled and coupled formulations. The only difference occurs in the second rows and concerns whether the equilibrium equation is formulated in terms of the classical stresses σ^c_{ij} (as per the uncoupled formulation of Ru and Aifantis) or the in terms of the gradient-enriched stresses σ^g_{ij} (following Eringen's uncoupled formulation).

The finite element implementations of the uncoupled and coupled formulations are treated in detail in (Askes et al., 2008) and in (Askes and Gutiérrez, 2006), respectively. The interpolations suggested in those studies will also be adopted here. For the uncoupled formulation we will use bilinear four-noded quadrilateral finite elements for the interpolation of the stresses and the displacements. The coupled formulation will be interpolated with quadratic eight-noded quadrilaterals for the stresses and bilinear four-noded quadrilaterals for the displacements. The latter discretisation must formally be verified against the inf–sup condition for mixed formulations, however this will be reported in a forthcoming contribution.

5. Numerical tests

Our aim now is to describe and analyse the behaviour of cortical bone in terms of stress profiles around cracks, taking into account the underlying microstructure via length scale parameters as suggested above. Two different scenarios will be considered, namely longitudinal and transverse tibial fractures, in order to verify the relevance and significance of the particular length scale parameter. Here longitudinal fracture is fracture along the fiber-like structures in the bone; and transversal fracture is fracture in the perpendicular plane, that is the plane of the Haversian systems. Figs. 2 and 3 provide details on geometry and boundary conditions. In both cases the specimens will be subjected to tension via imposing displacements $u = L/100$ in the longitudinal direction of the bone at the top of the specimens. Both cases will be modelled with the uncoupled and coupled gradient elasticity formulations, so as to verify whether both models can predict realistic results in case of anisotropic material.

5.1. Classical elasticity versus gradient elasticity

The need for gradient-enrichment is verified by comparing classical elasticity (obtained by setting $\ell_F = \ell_H = 0$) with the uncoupled version of gradient elasticity (used here via taking $\ell_F = \ell_H = 0.1$ mm). Note that here the gradient activity is isotropic but the material behaviour is still anisotropic through use of Eq. (15). A sequence of four recursively refined finite element meshes is used, consisting of 8×8 to 64×64 elements. Fig. 4 shows the vertical normal stress along the line $x_1 = 0$ for the various meshes. The results do not converge upon mesh refinement when classical elasticity is used, and instead unrealistic singular behaviour is observed. In contrast, the use of gradient elasticity renders results that converge towards a finite, smooth stress profile. The same trends are seen for the other stress components and in the coupled gradient elasticity model — these results are well-known and are therefore only briefly revisited here for the sake of completeness. In this connection, it is noted that certain analytical solutions of gradient elasticity that have appeared recently in the literature (e.g. Georgiadis, 2003; Karlis et al., 2007; Giannakopoulos et al., 2008) have deduced compressive stresses near the tip region which go to infinity when the crack tip is approached. In view of the present results and physical intuition such findings are difficult to accept. On the other hand such stress and strain singularities at the crack tip are removed if the extra boundary conditions associated with the higher order terms are more *agreeable* with physical intuition and expected *finite stress* behaviour at the crack tip and usual *classical* behaviour far away from it (Aifantis, 2009a; Aifantis, 2009b).

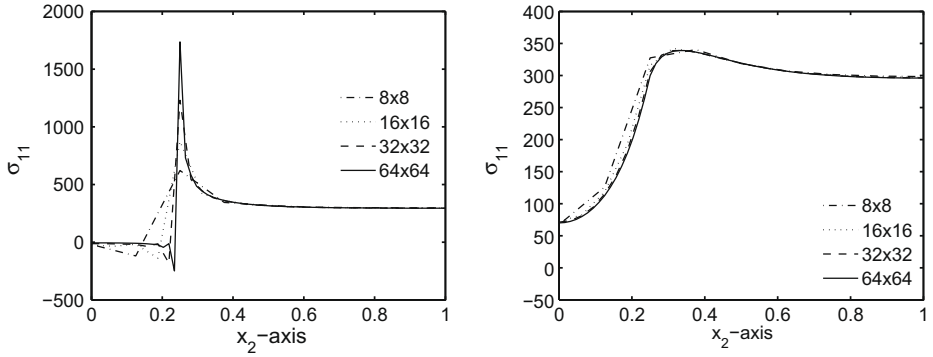

Fig. 4. Classical formulation with $\ell_F = \ell_H = 0$ (left) and uncoupled gradient elasticity with $\ell_F = \ell_H \neq 0$ (right).

5.2. Uncoupled versus coupled gradient elasticity

Next, we investigate the qualitative and quantitative differences between uncoupled and coupled gradient elasticity. Both models were tested with $\ell_F = \ell_H$. As mentioned above, two mechanically different scenarios are considered, i.e. transversal and longitudinal fractures. First the sample with transversal fracture is analysed. Fig. 5 shows the two normal stress components along the line $x_1 = 0$ for both gradient elasticity formulations. It can be seen that the two models behave qualitatively similar, although there are some quantitative differences: the coupled formulation is better capable to reproduce the zero tractions on the crack face. The reason may be that in the present analysis coupled formulation equilibrium and traction boundary conditions are enforced on these stresses, whereas the gradient-enriched stresses are not equilibrated in the uncoupled formulation but instead are obtained from solving Eq. (11). Both models show a good convergence upon refinement of the mesh. The case with longitudinal fracture is shown in Fig. 6, and the same observations hold.

Since the two formulations predict results that are qualitatively similar, in the remainder of this paper we will only show the results of the uncoupled formulation. However, the qualitative correspondence between the results of the two formulations was observed for all other tests reported upon below.

5.3. Transverse fracture

In this section and the next, anisotropy of the cortical bone will be treated not only via an anisotropic stiffness matrix, but also via using different length scale parameters, i.e. $\ell_F \neq \ell_H$. Transverse fracture of the bone is considered.

First, we will approximate the fibers to be infinitely long and parallel to each other, such that the material in the fiber-direction will be homogeneous. As a result, the longitudinal length scale $\ell_F = 0$. The results of this anisotropic model are presented in Fig. 7. These results are in a good agreement with those of the model with *isotropic heterogeneity* (i.e. the model where $\ell_F = \ell_H$,

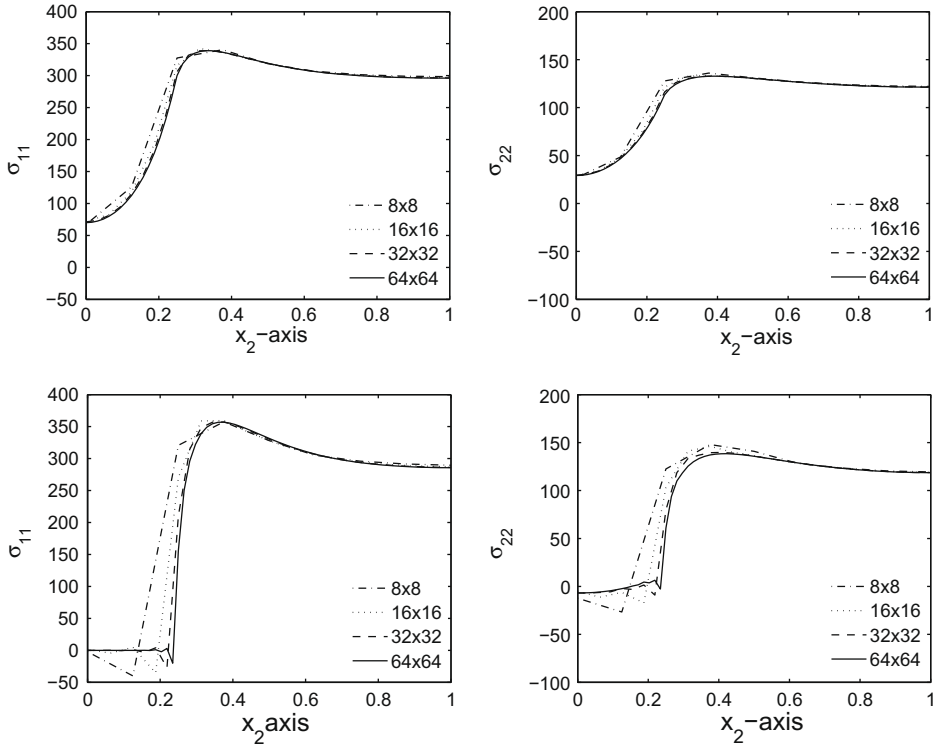

Fig. 5. Transversal fracture — horizontal (left) and vertical (right) normal stress for uncoupled (top) and coupled (bottom) gradient elasticity with $\ell_F = \ell_H$.

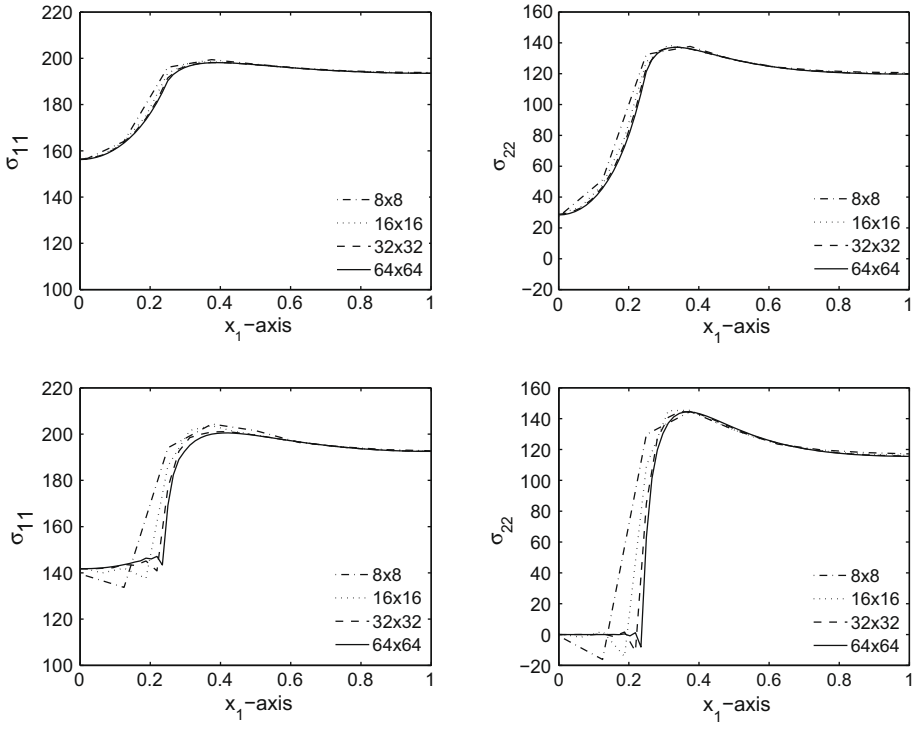

Fig. 6. Longitudinal fracture — horizontal (left) and vertical (right) normal stress for uncoupled (top) and coupled (bottom) gradient elasticity with $\ell_F = \ell_H$.

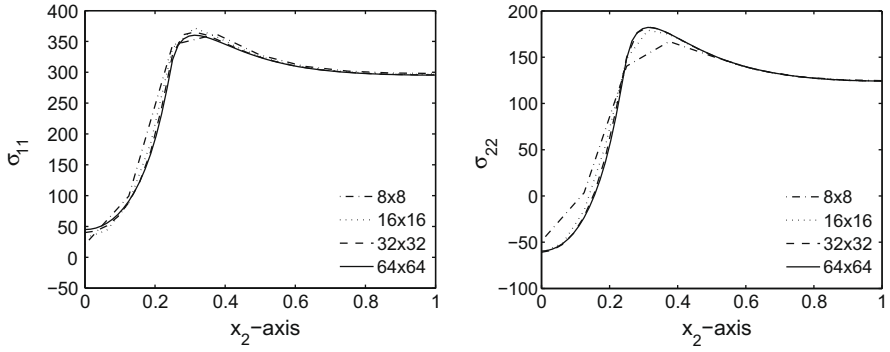

Fig. 7. Transversal fracture — horizontal (left) and vertical (right) normal stress; transverse heterogeneity activated via $\ell_H = l$ and $\ell_F = 0$.

see Fig. 5–top). As such, it can be concluded that the importance of the longitudinal heterogeneity via ℓ_F is secondary.

To validate this last statement, another test has been performed, namely including only longitudinal heterogeneity. The results of this test are obtained with $\ell_H = 0$ and $\ell_F = \ell$, and they are presented in Fig. 8. It is obvious from these results that the behaviour of the model now is quite different from our reference case of isotropic heterogeneity. Both normal stresses exhibit sharp spikes at the crack tip. This was also observed in classical elasticity. However, it should be noted that the results of Fig. 8 converge to finite

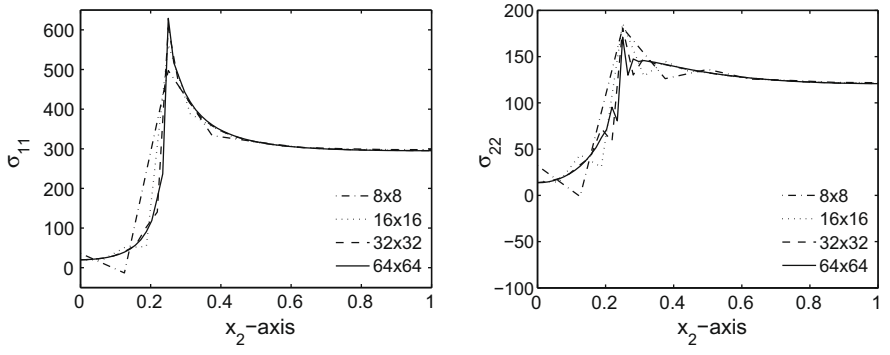

Fig. 8. Transversal fracture — horizontal (left) and vertical (right) normal stress; longitudinal heterogeneity activated via $\ell_H = 0$ and $\ell_F = l$.

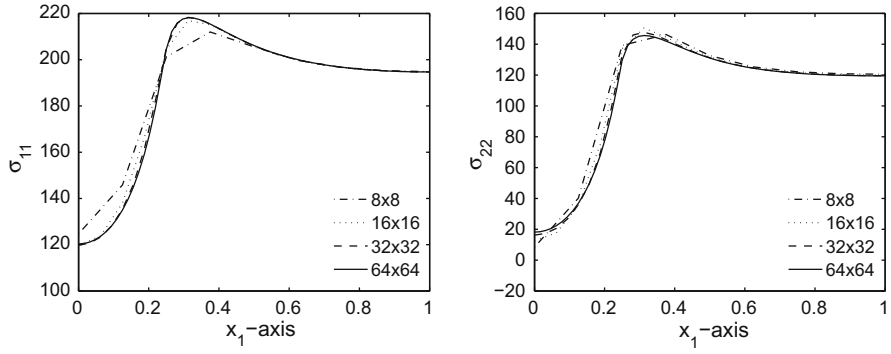

Fig. 9. Longitudinal fracture — horizontal (left) and vertical (right) normal stress; longitudinal heterogeneity activated via $\ell_H = 0$ and $\ell_F = \ell$.

values. This conclusion is based on Richardson extrapolation (Burden and Faires, 2001) of the stress values at the crack tip. The extrapolation shows that the results of classical elasticity converge to very large stresses, which is interpreted as approaching infinity. Conversely, in the case of accounting for anisotropic gradient activity the extrapolated solutions are finite numbers, and these numbers are just marginally larger than the results obtained with the finest mesh. Thus, there is an important difference between the *spiky, yet converging stresses* observed in Fig. 8 and the *spiky, singular stresses* shown in Fig. 4–left.

5.4. Longitudinal fracture

Next, we consider longitudinal fracture (see Fig. 2) by firstly taking the heterogeneity is taken to be dominant in the longitudinal direction (that is, $\ell_H = 0$ and $\ell_F = \ell$). The results of this model are presented in Fig. 9, and they are in good agreement, qualitatively and quantitatively, with the results of the model with isotropic heterogeneity (see Fig. 6–top). This leads to the conclusion that the longitudinal heterogeneity is the dominant one in case of longitudinal fracture.

Again, this statement is verified by taking transverse heterogeneity via $\ell_H = l$ and $\ell_F = 0$. These results are presented in Fig. 10. The observations and conclusions of this test follow closely the case of transversal fracture with longitudinal heterogeneity: sharp spikes occur in the stress profiles, but the results seem to converge to finite, non-singular values.

6. Conclusions

The main purpose of this paper is to offer a reliable, yet simple model that can be used to simulate stress concentrations in fractured cortical bone. Multiscale modelling approaches are appropriate choices in order to capture the interaction between the microstructure and the macroscopic geometry under given loading conditions. Among the vast amount of multiscale techniques known in the literature, *gradient elasticity* stands out for its conceptual simplicity, its mathematical elegance and its flexibility in describing a wide range of phenomena. Gradient elasticity models ensure realistic mechanical behaviour by introducing extra gradient terms accompanied by length scale parameters that carry the information about the lower scale structure of the material. Two different gradient elasticity formulations were used in this study. The two versions show qualitatively similar results, but the formulation due to Ru and Aifantis is simpler in terms of computer implementation and less expensive in terms of computer run-time, since it is an *uncoupled* formulation.

The complexity of bone modelling arises with bone being a highly anisotropic material: in the longitudinal direction bone has a fiber-like structure and in the transversal plane it has a structure of Haversian systems. As such one more requirement is put on the modelling strategy: it has to be able to describe such an anisotropy. In gradient elasticity, anisotropy is accounted for twofold. Firstly, the effective elastic stiffness properties (Young's modulus, Poisson's ratio) can be taken to be anisotropic, as is well-established. Secondly, the concept of *anisotropic heterogeneity*, as manifest by gradient activity, can be adopted by choosing the length scale parameters to be different in different spatial directions.

The choice of these length scale parameters is a separate and complicated task, and it has been addressed in various studies in the literature. It can be quite an expensive and ethically challenging task as well while testing human bones. Thus, a simplification of the model has been suggested here: dominant and secondary directions of interest are to be distinguished, with the idea that only the length scale in the dominant direction is to be used and quantified. This last approximation requires a thorough testing and we have carried out numerical simulations to support this approximation.

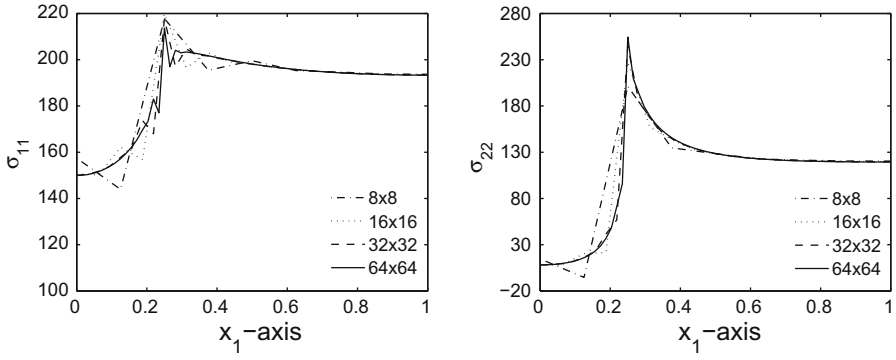

Fig. 10. Longitudinal fracture — horizontal (left) and vertical (right) normal stress; transverse heterogeneity activated via $\ell_H = l$ and $\ell_F = 0$.

Two different scenarios of fracture were considered: fracture in the longitudinal direction and fracture occurring in the transversal plane. These two fracture scenarios are combined with two assumptions on the dominant direction of heterogeneity, namely longitudinal (whereby the fibers are supposed to be the main source of heterogeneity) and transversal (where heterogeneity is caused by the Haversian systems). All of the above tests support the overall conclusion that it is sufficient to include only one length scale, namely the length scale in the direction of the considered fracture. In other words, it is sufficient to validate the microstructural information of the bone in the direction of the fracture only. This is an important observation, since it might not be straightforward to measure (experimentally or deduce by other possible means) the effective properties (for example the representative volume element) of a human bone. With only one length scale required, rather than two, this task becomes twice as easy.

Acknowledgments

We gratefully acknowledge financial support of the European Commission (RTN DEFINO HPRN-CT-2002-00198, *Deformation and fracture instabilities in novel materials and processes*). The first author acknowledges financial support of the Engineering and Physical Sciences Research Council of the United Kingdom (Grant number EP/D041368/1). The second author also acknowledges support from the US Government through NSF/NIRT Grant DMI-0532320, as well as the Greek Government through PENED and PYTHAGORAS programs. The authors also acknowledge the very useful remarks and suggestions of the reviewer.

References

Aifantis, E.C., 1992. On the role of gradients in the localization of deformation and fracture. International Journal of Engineering Science 30, 1279–1299.
Aifantis, E.C., 1994. Gradient effects at macro, micro and nano scales. Journal of the Mechanical Behavior of Materials 5, 355–375.
Aifantis, E.C., 1999. Strain gradient interpretation of size effects. International Journal of Fracture 95, 299–314.
Aifantis, E.C., 2003. Update on a class of gradient theories. Mechanics of Materials 35, 259–280.
Aifantis, E.C., 2009a. Exploring the applicability of gradient elasticity to certain micro/nano reliability problems. Microsystem Technologies 15, 109–115.
E.C. Aifantis, On scale invariance in anisotropic plasticity, gradient plasticity and gradient elasticity, International Journal of Engineering Science. doi: 10.1016/j.ijengsci.2009.07.003.
Altan, B.S., Aifantis, E.C., 1997. On some aspects in the special theory of gradient elasticity. Journal of the Mechanical Behavior of Materials 8, 231–282.
Askes, H., Aifantis, E.C., 2002. Numerical modeling of size effects with gradient elasticity — formulation meshless discretization and examples. International Journal of Fracture 117, 347–358.
Askes, H., Gutiérrez, M.A., 2006. Implicit gradient elasticity. International Journal for Numerical Methods in Engineering 67, 400–416.
Askes, H., Morata, I., Aifantis, E.C., 2008. Finite element analysis with staggered gradient elasticity. Computers and Structures 86, 1266–1279.
Bažant, Z.P., Novák, D., 2003. Stochastic models for deformation and failure of quasibrittle structures: recent advances and new directions. In: Bićanić, N., de Borst, R., Mang, R., Meschke, G., (Eds.), Computational Modelling of Concrete Structures.
Burden, R.L., Faires, J.D., 2001. Numerical Analysis, seventh ed. Brooks/Cole.
Drugan, W.J., Willis, J.R., 1996. A micromechanics-based nonlocal constitutive equation and estimates of representative volume element size for elastic composites. Journal of the Mechanics and Physics of Solids 44, 497–524.
Eringen, A.C., 1983. On differential equations of nonlocal elasticity and solutions of screw dislocation and surface waves. Journal of Applied Physics 54, 4703–4710.
Eringen, A.C., 2002. Nonlocal Continuum Field Theories. Springer-Verlag, New York.
Fatemi, J., van Keulen, F., Onck, P.R., 2002. Generalized continuum theories: application to stress analysis in bone. Meccanica 37, 385–396.
Georgiadis, H.G., 2003. The mode III crack problem in microstructured solids governed by dipolar gradient elasticity: static and dynamic analysis. Journal of Applied Mechanics 70, 517–530.
Giannakopoulos, A.E., Stamoulis, K., 2008. Size effects on strength, toughness and fatigue crack growth of gradient elastic solids. International Journal of Solids and Structures 45, 4921–4935.
Gitman, I.M., Askes, H., Aifantis, E.C., 2005. The representative volume size in static and dynamic micro-macro transitions. International Journal of Fracture 135, L3–L9.
Gitman, I.M., Askes, H., Sluys, L.J., 2007. Representative volume: existence and size determination. Engineering Fracture Mechanics 74, 2518–2534.
Gutkin, M.Y., 2000. Nanoscopics of dislocations and disclinations in gradient elasticity. Reviews on Advanced Materials Science 1, 27–60. Also available at: http://www.ipme.ru .
Gutkin, M.Y., Aifantis, E.C., 1999. Dislocations in the theory of gradient elasticity. Scripta Materialia 40, 559–566.
Hoffmeister, B.K., Smith, S.R., Handley, S.M., Rho, J.Y., 2000. Anisotropy of Young's modulus of human tibial cortical bone. Medical and Biological Engineering and Computing 38, 333–338.
Karlis, G.F., Tsinopoulos, S.V., Polyzos, D., Beskos, D.E., 2007. Boundary element analysis of mode I and mixed mode (I and II) crack problems of 2-d gradient elasticity. Computer Methods in Applied Mechanics and Engineering 196, 49–52.
Kirchner, H.O.K., Lazar, M., 2008. The thermodynamic driving force for bone growth and remodelling: a hypothesis. Journal of the Royal Society Interface 5, 183–193.
Lakes, R.C., 1983. Size effects and micromechanics of a porous solid. Journal of Materials Science 18, 2572–2581.
Lakes, R.C., 1986. Experimental microelasticity of two porous solids. International Journal of Solids and Structures 22, 55–63.
Lazar, M., Maugin, G.A., 2005. Nonsingular stress and strain fields of dislocations and disclinations in first strain gradient elasticity. International Journal of Engineering Science 43 (13–14), 1157–1184.
Lazar, M., Maugin, G.A., Aifantis, E.C., 2005. On dislocations in a special class of generalized elasticity. Physica Status Solidi (b) 242, 2365–2390.
Mindlin, R.D., 1964. Micro-structure in linear elasticity. Archive for Rational Mechanics and Analysis 16, 51–78.
Mindlin, R.D., 1968. Theories of elastic continua and crystal lattice theories. In: Kroener, E. (Ed.), Mechanics of Generalized Continua IUTAM Symposium. Springer, Berlin, pp. 312–320.
Mindlin, R.D., 1972. Elasticity, piezoelasticity and crystal lattice dynamics. Journal of Elasticity 2 (4), 217–282.
Mindlin, R.D., Eshel, N.N., 1968. On first strain-gradient theories in linear elasticity. International Journal of Solids and Structures 4, 109–124.
Ren, Z.-Y., Zheng, Q.-S., 2002. A quantitative study of minimum size of representative volume elements of cubic polycrystals – numerical experiments. Journal of Physics of Solids 50, 881–893.
Rho, J.Y., 1996. An ultrasonic method for measuring the elastic properties of human tibial cortical and cancellous bone. Ultrasonics 34, 777–783.
Ru, C.Q., Aifantis, E.C., 1993. A simple approach to solve boundary-value problems in gradient elasticity. Acta Mechanica 101, 59–68.
Tenek, L.T., Aifantis, E.C., 2002. A two-dimensional finite element implementation of a special form of gradient elasticity. Computer Modeling in Engineering and Sciences 3, 731–741.